



Journal of Applied and Computational Mechanics



Research Paper

Finite Elements Analysis of the Hyperelastic Impeller Rotating in the Self-Priming Pump

Ana Pavlovic

Department of Industrial Engineering, Alma Mater Studiorum University of Bologna, Via Fontanelle 40, 47121, Forlì, Italy

Received January 13 2022; Revised March 02 2022; Accepted for publication March 04 2022.

Corresponding author: A. Pavlovic (ana.pavlovic@unibo.it)

© 2022 Published by Shahid Chamran University of Ahvaz

Abstract. Volumetric self-priming pumps with deformable impeller blades are very common devices in the food industry, especially in the presence of viscous liquids that tend to foam or contain suspended solids, but also when working under vacuum with good suction capacity is needed. These pumps are characterized by a circular chamber with an eccentric, in which the impeller rotates: due to the continuous deformation of flexible blades, the liquid is moved up to the discharge. The exact evaluation, moment by moment, of the hyperelastic behaviour of the impeller represents a quite complex task, involving several miscellaneous phenomena. In this study a simplified quasistatic analysis by finite element discretization is proposed, able to evaluate with reasonable approximation the stress/strain state of the impeller blades during their rotation. Aspects such as material hyperelasticity, large displacements, large deformations, non-linearity in contacts, frictional and inertial forces were considered.

Keywords: Self-priming pumps; Flexible Impeller Pumps (FIPs); impeller blades; non-linearity; hyperelasticity; contacts.

1. Introduction

Choosing a pump for wine making may be less simple than it seems. In this regard, Phillips introduced his recent work on pumps for moving juice, must and wine with a representative statement [1]: 'When I am asked to recommend pumps for wineries, the conversation usually becomes much more protracted than expected'. It is surprising 'when something as apparently straightforward as a pump can become the subject of a drawn-out discussion'.

Indeed, the advice on the choice of such pumps is lost in the mists of time. Browsing through the historical archives, as early as the first half of the 1800s, for instance, Hilton proposed a series of short articles with the scope to teach how to choose the proper pump for racking wine [2, 3].

Compared to those far years, the current technologies have changed a lot as well as the methods for understanding the behaviour of these pumps: not only preliminary calculations and experiments, but also numerical models. However, it is not easy to find specific articles dealing with wine pumps [4], and it is therefore necessary to import methods and results taken from other investigation fields.

Limiting the present analysis to self-priming pumps, as defined, and largely described in [5], the self-priming process of multistage self-priming centrifugal pump was, for instance, numerical simulated by ANSYS CFX software in [6]. The model considered gas-water two-phase flow on a four-stage self-priming pump and experimental results were very close to the predictions especially in the initial and middle self-priming stages. This work is almost representative of many others available in literature that, similarly, use the Computational Fluid Dynamics (CFD) as modelling approach. By the same authors, for instance, another work detailed a method to optimize a typical multistage centrifugal pump based on energy loss model and CFD [7]. This optimisation can be also addressed to the design of impellers and blades, as in [8-11] where several shapes and materials were considered and compared or in [12] where blades trimmers were evaluated as a way for improving pump efficiency.

Besides, design procedures assume a distinctive complexity in the presence of solid-liquid suspensions, moved by a rigid-flexible impeller [13, 14], characterized by a significant hyperelasticity in materials properties [15]. This is the case of wine self-priming pumps under examination here.

We refer to the Flexible Impeller Pumps (FIPs), an important class of compact, versatile, and simple pumps thanks to the presence of a single moving part and no gears. They are used to handle fluid or viscous liquids, even in the presence of suspended solid bodies and in both flow directions. For such a purpose, the FIPs adopt a deformable impeller rotating inside a chamber characterized by a proper geometry to generate the suction, displacement, and discharge effects on the fluid. During the rotation of the impeller, the eccentric shape of the pump chamber is such as to deform the blades present in the suction section and lead to their greater spacing. This creates an increase in the free volume between two adjacent blades, which is immediately filled by the fluid. The further step of rotation of the impeller carries the fluid from the suction section to the discharge section where, again due to the shape of the pump body, the blades relax in part, reducing the free volume and causing the fluid to drain. The rapid succession of the blades, with their sliding always in contact with the walls of the pump body, creates a uniform flow of fluid (Fig. 1).



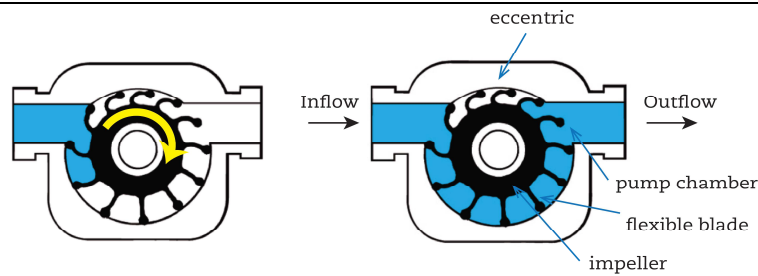


Fig. 1. Operating principle of a flexible impeller pump.

An impeller in neoprene is traditionally mounted in these pumps, but other natural or synthetic rubbers are also frequently considered as, e.g., in the case of nitrile, preferred in the presence of aggressive chemical agents. Ethylene-Propylene Diene Monomer (EPDM) is often selected due to its valuable material properties. EPDM offers, for instance, a marked resistance to heat, ozone and atmospheric agents, together with excellent electrical insulation properties. Moreover, thanks to vulcanization, it even exhibits valuable mechanical properties, which can be determined by a suitable choice of compound and processes, such as hardness of 40-90 Shore A, tensile strength of 25 MPa and density between 0.9 and 2.0 g/cm³ [16-18].

These hyperelastic materials permit to work liquid foaming with an amount important of solids in suspension as in the case of, e.g., de-stemmed grapes, which can be pumped without causing stopping or seizure of the rotating part.

Adjustments in rotary by means of a speed variator permit to modify the flow (from 22 to 830 litres/minute). At very low speed they are suitable for the transfer of very dense liquids. Generally, they are mounted under the crusher, or they are used for pumping over with marc.

However, after a few years of use it becomes necessary to replace the impeller anyway. They are commonly designed, in fact, to last 3000-4000 hours, equal to 2- or 3-years operation in the case of a use 'traditional', i.e., at temperature ambient and up to 400 rev / min. To achieve the presented target, it is necessary to pay attention to different aspects of the design such as fatigue resistance, wear and much more. In this optic, it can already be considered an important target the development through a quasistatic approach, as here proposed, of a first discretization model able to predict the structural behaviour (i.e., stress/strain) of blades and impeller during their motion.

2. Materials and Methods

2.1 System

The Flexible Impeller Pump (FIP) under investigation is designed and manufactured by Francesca Wine Pumps Srl in Imola. It is part of a group of oenological pumps, patented as Caterina®, containing a flexible, dry self-priming impeller, with parts in contact with the liquid entirely in stainless steel. The specific geometry guarantees an immediate suction capacity, even when dry, with priming up to a depth of 7 meters. The engine also allows a soft pumping, with continuous and regular flows. The conformation of the flexible impeller provides the ability to treat viscous liquids even in the case of suspended bodies. The pump body is molded in a single piece, from thick stainless-steel sheet (AISI 316), synonymous with quality and durability. The pump bodies are subjected to constant quality control of the welds and are internally and externally polished to offer maximum hygiene. The impeller is extracted from synthetic rubber, EPDM (instead of Neoprene), non-toxic and resistant to several acids. The most relevant technical data are reported in Table 1 highlighting the values of maximum internal pressure (3.0 bar) and rotor rotational speed (between 30 and 400 rpm) that were used in the model definition.

2.2 Materials properties

In line with technical characteristics, the following assumptions were done on materials properties:

- 1) circular chamber made by stainless steel, characterized by an elastic behaviour ($E = 200$ GPa)
- 2) a deformable impeller, in ethylene-propylene-diene (EPDM)
- 3) characterized by an hyperelastic Neo Hookean behaviour [19]
- 4) included in the calculation by inserting the experimental stress/strain curves (Fig. 2)
- 5) two different formulations of compound were compared. They properties were detected by experiments:
 - DA1104, in certified clear rubber, with hardness of 59 (Shore A, at fixed load), very high elastic yield (70% at the Zerbini pilinbalometer) with deformation of 100% to 1.9 MPa, 200% at 2.2 MPa, 300% at 3.6 MPa and breaking at 550% for 12.2 MPa.
 - FP1161, in FDA certified black rubber, with hardness 63 (Shore A), average elastic yield (58% at Zerbini pilinbalometer) with deformation of 100% at 3.7 MPa, 200% at 6.6 MPa, 300% at 10.1 MPa up to 320% failure for 11.5 MPa.

Table 1. Technical characteristics (Mod. C20).

Characteristics	Values
Scope	4,600 - 22,000 l / h
Recommended minimum fitting	Ø60
Typology	flexible impeller
Max working pressure	3.0 bar
Rotation speed	80 - 400 rpm
Motor	2.2 kw
Ampere	5.1
Variator	Electronic
Voltage	380/480 Three-phase
Frequency	50/60 Hz
Pump body material	AISI 316
Piston / rotor material	EPDM
Gaskets	Graphite - Ceramic
Weight	88.0 Kg
Size	79 x 57 x 90 cm



Table 2. Mechanical properties of materials.

Property	Unit	Room	Impeller	
Material		Steel	EPDM	
Type		AISI 316	DA1104	FP1161
Density	kg/m ³	7850	1230	1400
Elastic module	MPa	200 000	2,000	3700
Poisson's ratio	-	0.30	0.33	0.33
Yield Strength	MPa	250	-	-
Break Resistance	MPa	460	12.2	11.5
Elongation at Break	%	40-45	550	320

These properties are summarized in Table 2.

2.3 Discretization

For the proper numerical model definition, it was necessary to consider to be in the presence of

- a dynamic problem \Rightarrow large displacements
- sliding frictional contacts \Rightarrow non-linear contacts
- highly deformed non-elastic materials \Rightarrow non-linear materials, large displacements
- irregular geometries \Rightarrow high number of discretization nodes, low computing efficiencies
- pre-stressed/deformed geometries \Rightarrow initial interpenetration between bodies

Regarding the last-mentioned aspect, it is related to the fact that the impeller encounters an initial geometrical deformation due to interference during assembly (Fig. 3). Therefore, this part' geometry had to be properly deformed before including in the numerical model.

Consequently, for a better convergence of algorithms, the following assumptions and simplifications were provided:

- Physical model

1) Elimination of the upper half of the impeller (A-A symmetry plane) and the lower half of the pump body (B-B symmetry plane).

2) Initial rotation of the impeller to create an initial contact condition.

In other words, to solve the problem of initial interpenetration and lack of contact between the impeller and the chamber, the system was reduced into two half-parts, not in contact with each other (Fig. 4a). The subsequent imposition of rotation of a specific angle (14.76°) made it possible to bring the first blade into initial contact with the pump body (Fig. 4b), ready to be progressively deformed until it assumes that deformed configuration that it has in the pump for assembly. Since explained problem is studied as a quasi-static model, the viscoelastic properties of the material of which the flexible impeller is made are not so relevant. They would become fundamental in a full-dynamic analysis, for the evaluation of first-contact impact forces of the blades, and consequent relaxation of the material which will be taken into account in future analyses.

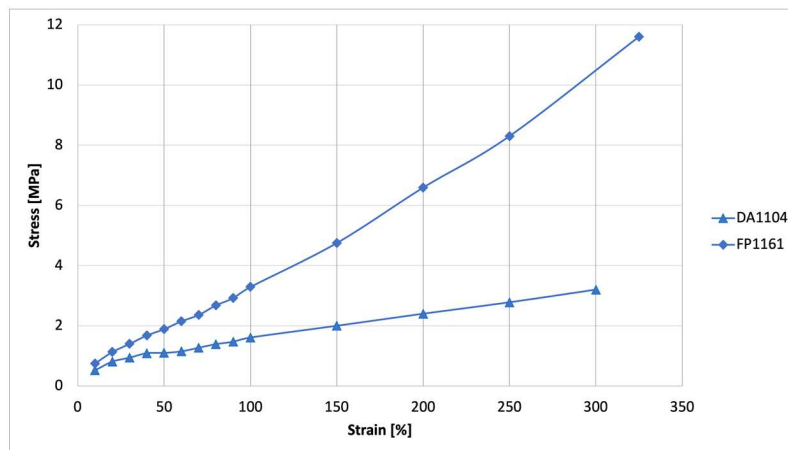


Fig. 2. Hyperelastic behaviour of selected EPDM.

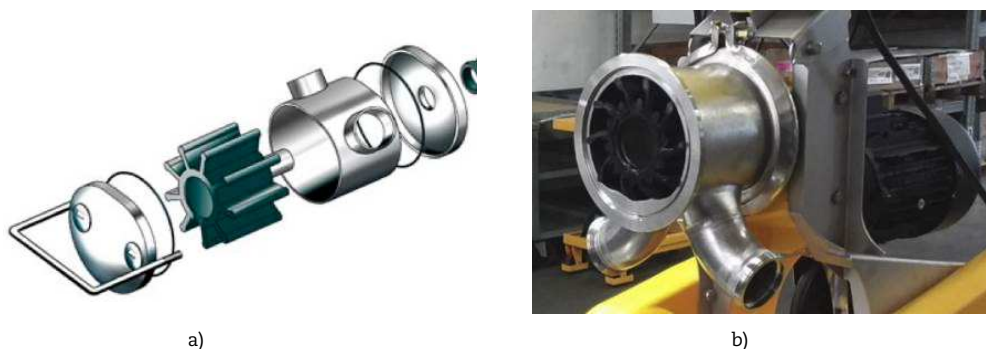


Fig. 3. Flexible impeller pump: a) simplified exploded diagram; b) assembled system with deformed impeller.



- Type of analysis

- 3) Modeling the physical system by means of quasistatic structural analysis and no longer stationary fluid-dynamics.
- 4) Conversion of dynamic conditions (angular velocity: 30rad/s) into static conditions through (Fig. 4b):
 - a. the application of an imposed rotation.
 - b. the application of a static force equivalent to the centrifugal force

The imposed rotation was applied at a certain value of angular speed (30 rad/s). In other words, the effect on the blades of a quasistatic rotation of defined angles was studied. These angles were chosen in the way to allow at least one or more blades to pass through the eccentric and thus undergo the complete cycle of bending and relaxation. The centrifugal force linked to the rotational motion, which pushes the blade against the pump body (also increasing friction), was included in the calculation. Since quasi static simulation is performed impact forces and viscoelastic properties of the model were not considered in this stage.

- External conditions

- 5) Structure constrained in such a way as to prevent any displacement or rotation with respect to any direction. This condition was applied to each node of the internal surfaces of the circular chamber.
- 6) Fluid-dynamic effect of the transferred liquid, simplified as a constant pressure on one face of the blades and equal to 3 bar (Fig.4c).
- 7) Frictional contact between the pump chamber and impeller surfaces (blue and red in Fig. 5), with a friction coefficient of 0.1 [20, 21].

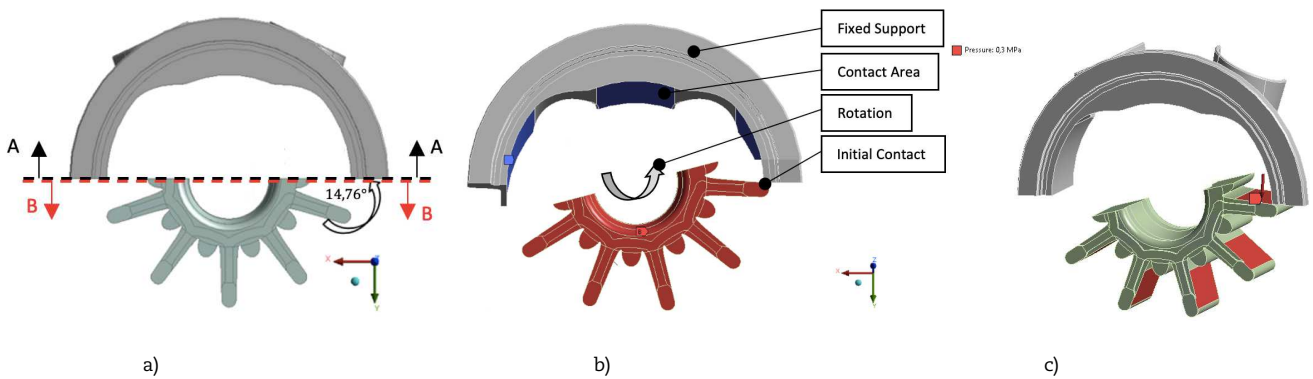


Fig. 4. Modeling assumptions by application of: a) symmetries and initial contact; b) load and constraints; c) pressure and forces.



Fig. 5. Details on contact surfaces, between the deformable impeller (red) and the fixed pump body (blue).

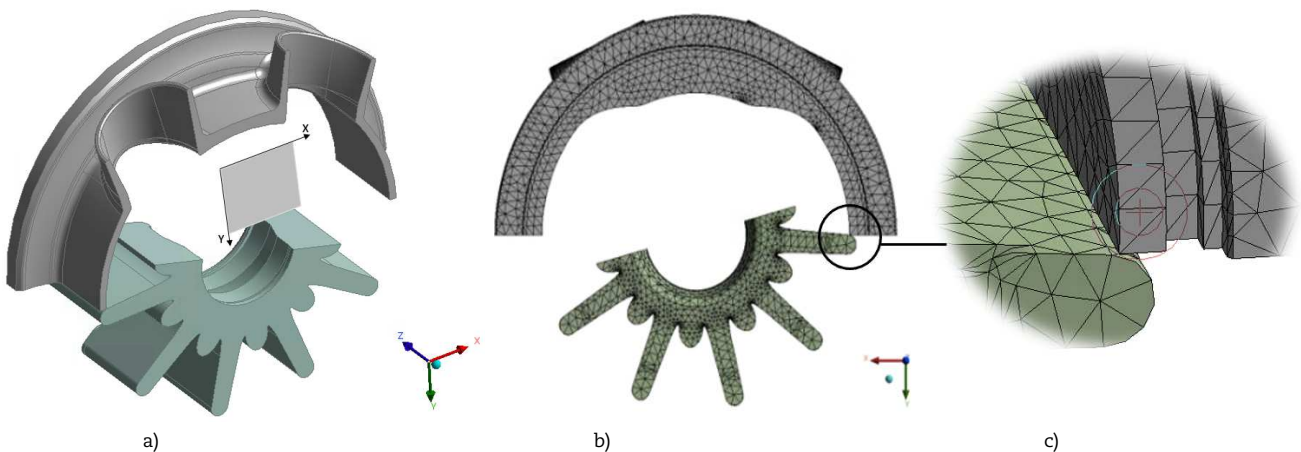


Fig. 6. Geometrical discretization by the application of symmetry (XY plane) and finite elements (Solid186).



- Discretization

8) Use of *Solid186* as finite elements that is a tetrahedral homogeneous structural solid element with 20 nodes, with 3 degrees of freedom (X, Y, Z nodal translations) each. This element, which shows a quadratic displacement behaviour, was chosen considering it can support phenomena of plasticity, hyperelasticity, sliding, stiffening from deformation, large deflections, and deformations. Chosen finite element illustrate good stability regarding hourglass energy. Furthermore, in addition to being usable for any spatial orientation, useful for modelling irregular meshes [22, 23], it also has the capacity of mixed formulation that allows to simulate deformations of almost incompressible elastoplastic materials and completely incompressible hyperelastic materials [24, 25].

9) Application of a XY transversal symmetry plane (Fig. 6a) which allowed to halve the thickness of the system and the number of finite elements necessary for the discretization up to a mesh of 282947 nodes and 184001 elements of dimensions <5 mm, thickened in the contact areas (Fig. 6b,c).

3. Results and Discussion

3.1 Pre-stressed conditions

As first, the deformation effect of the blades due to the assembly phase was analysed. Figs. 7 and 8 show this fact and how displacements (mm) and strains (mm/mm) increase during the placement of impeller in the pump chamber. Displacement in this case can be understand as changing of position of the singular blade. It is equivalent to a forced rotation of 12.5° . When finally installed, a total displacement of 27 mm and strain of 0.165 mm/mm for blades are evident. In Fig. 7 it is also possible to notice a non-uniformity of the stress and strain states along the z direction until achieving the maximum values on the XY symmetry plane.

3.2 Stress and strain

The quasistatic structural simulation made it possible to evaluate the stress and strain states of the impeller for each position of interest. Fig. 9 shows, e.g., the values of (Von Mises) stress and strain of blades (in DA1104) in the case of an impeller rotation of 120° . This angle was chosen with the scope to allow a direct comparison between blades' states during their motion through the pump chamber. Considering blades in clockwise order, the first one have just passed the point of maximum shrinkage of the chamber, which is now engaged by the second blade. The third blade, on the other hand, is starting to approach the geometrical discontinuity, while the fourth has been just shaped by the initial deformation due to the assembly process, very different from the free profile still enjoyed by the fifth blade.

During this evolution, the blade is affected by a progressive increase in the stress level (passing from position 5 to 1), accompanied by an increase in deformations. Both are prevalent on the front section (with respect to the direction of rotation) of the blade and almost negligible (especially stresses) on the back one. The internal part of the impeller is much lower stressed than blades. A line of stress concentration appears on the bottom land, especially when the blade is near the middle of the eccentric. The stress state of a blade does not affect the adjacent one. No contact phenomena emerge between blades or between blades and the internal part of the impeller: these conditions are essential for a correct pump's functionalities. Internal part of the impeller, rounded 'teeth' between blades, are insert with the scope to reduce dead space between blades, with the reason to avoid changing in the pressure of the pump.

By a deeper analysis of results, it is also possible to detect a nonuniform stress / strain state respect to the rotation axis (i.e., Z axis), due to the surfaces irregularity in the area of the eccentric that produces a slight torsion in the blades (Fig. 10a). This is evident, in particular, in comparing the first twisted blade with and second untwisted blades. This twist, which is mirrored in the symmetrical part of the impeller (XY plane of symmetry) shapes the blade as an arc while passing through each of the two pump's inflow and outflow openings. Finally, in the same Fig. 10, it is easy to observe how the volumetric spaces between blades change according to their position creating that effect which characterizes FIPs.

Regarding the experimental validation, although it has not yet been possible to carry out direct strain measurements in the way to confirm the goodness of the numerical model, a visual comparison seems to indicate physical reality does not depart significantly from predictions. As reported in Fig. 11, in both cases, for example, no contact is evident between the blades or between the blades and the geometrical reinforcement between the grooves. Moreover, curves and distances also seem rather similar.

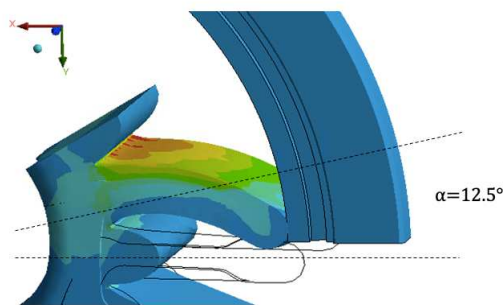


Fig. 7. Blade deformation during the phase of impeller installation.

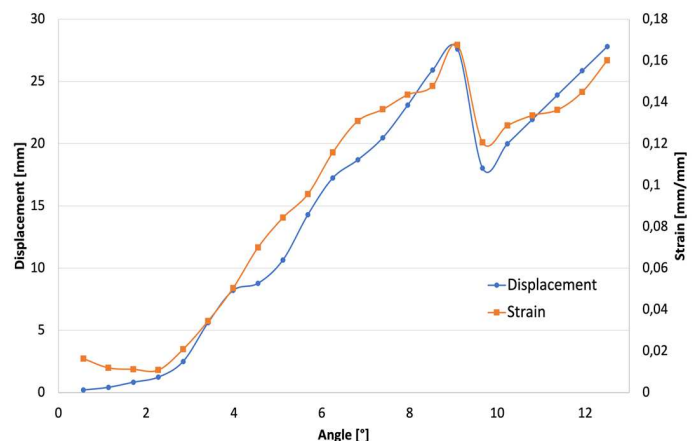


Fig. 8. Trends of strain and displacement during the impeller installation.



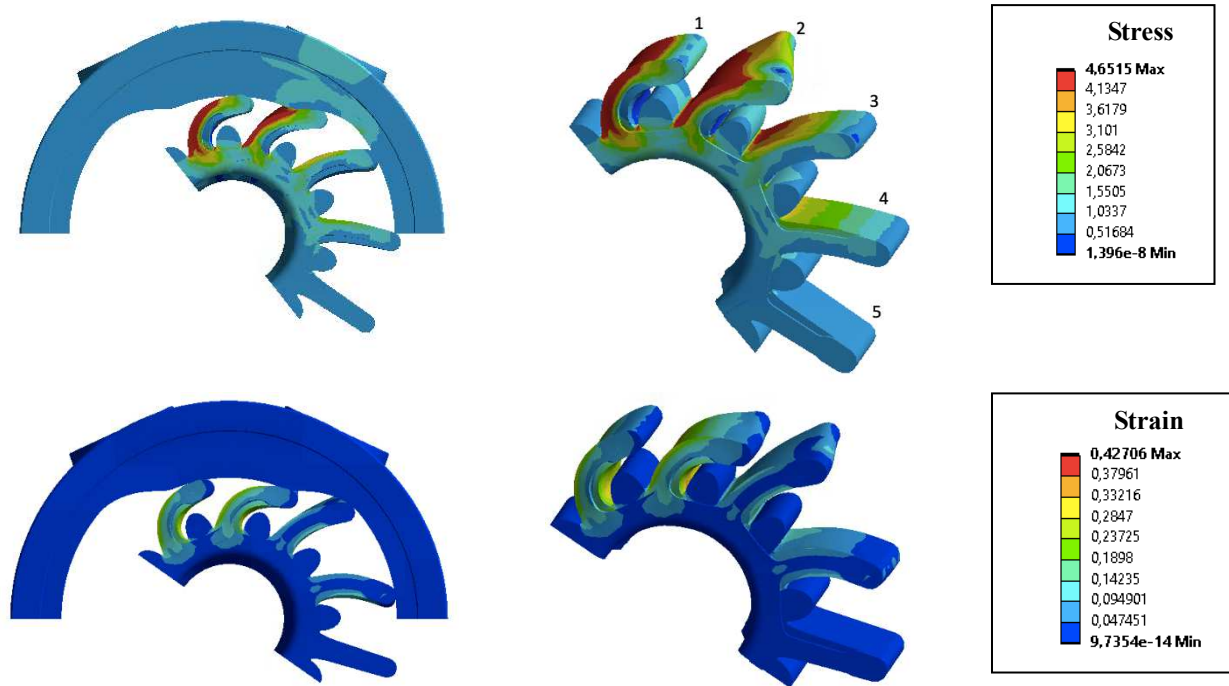


Fig. 9. Equivalent Von Mises stress, in MPa (up) and total strain, in mm/mm (down).

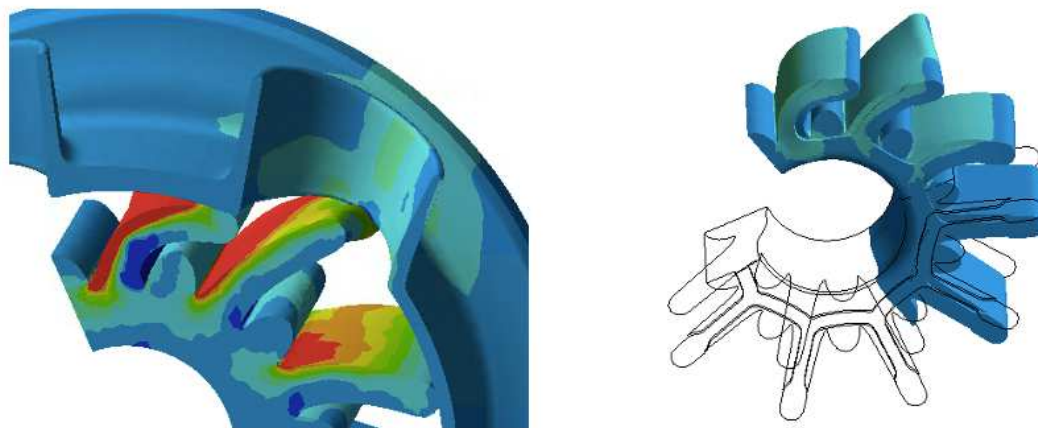


Fig. 10. Twisting effect due to the eccentric: comparing the first (twisted) and second (untwisted) blades.

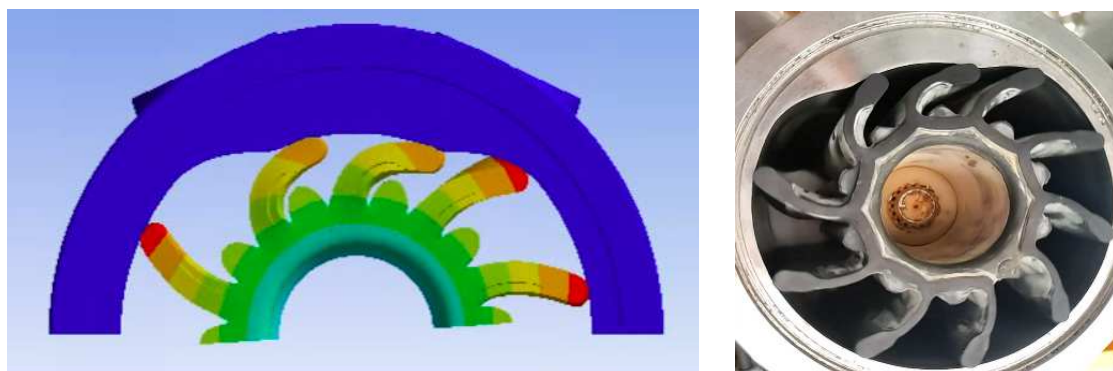


Fig. 11. Visual comparison between simulation and real respect to blades in the different stages.

3.3 Direct motion

The phenomena accruing during the direct motion of the impeller was studied by applying a rotation of 240° that permits all blades entering in the chamber. Some phases of this movement are represented in fig. 12 in terms of stress and strain. Their trends are reported in fig. 13, extracted from Ansys by selecting time and respectively stress and strain as a new diagram.



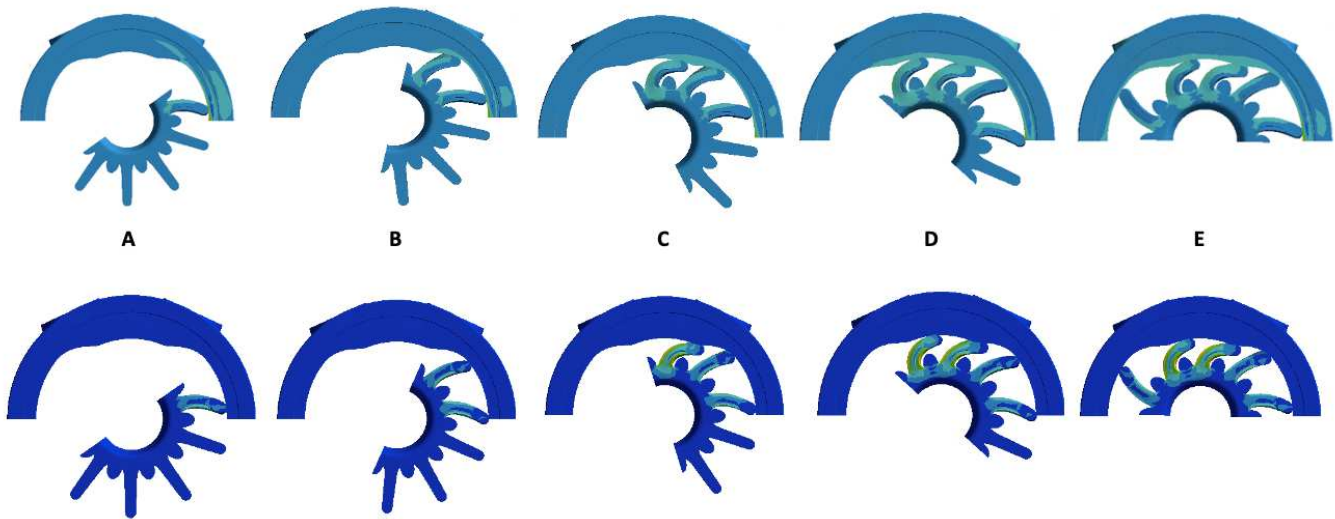


Fig. 12. Stress (up) and strain (down) respect to representative positions.

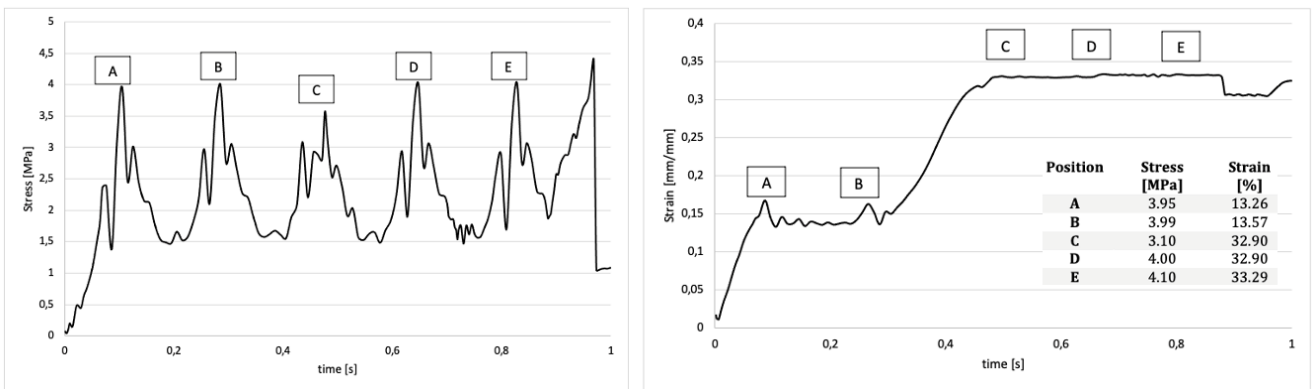


Fig. 13. Equivalent (Von Mises) stress and strain during the impeller rotation.



Fig. 14. Phases of reversal of direction.

Specifically, it is possible to confirm an initial pre-stressed state (A) of blades, already discussed, of 13.5% as strain and 1.50 MPa as stress. Then, these values increase while passing through the eccentric (B) up to, respectively, 33% (+150%) and 4.10 MPa (+170%). The fact that the deformation is more marked with respect to stress is linked to the high hyperelasticity of EPDM. The same sequence is repeated with the passage of the following blades (C,D,E) with stress and strain that alternated between the maximum and minimum indicated.

3.4 Inverse motion

An addition simulation aimed at investigating the effect of an inversion of the movement. It was simulated rotating the impeller from 0° to 120°, a condition that allowed the first blade to cover a good part of the discontinuity section of the pump body, and then inverting the movement rotating from 120° to 0°. This condition, quite common in real applications (Fig.14), given the possibility of using the pump with respect to both pumping directions, and like that were considered worthy for further investigation (Fig. 15).

Also in terms of deformations, the values calculated by the model, never higher than 35-40%, always remained very far from the expected deformations at break of 550% and 320% respectively (Table 3). Specifically, Fig. 16a relates the trend of the maximum values of tension (main) and deformation in the first blade. Fig. 16b instead compares the trends of the maximum deformation values with respect to the specific contact lines present in the top and bottom lands of the blade.



Table 3. Maximum values of stress and strain for two different impeller configurations.

		Direct Motion		Inverse Motion	
		DA1104	FP1161	DA1104	FP1161
Maximum Equivalent (Von Mises) stress	MPa	3.6	4.1	2.6	4.6
Maximum Principal Stress	MPa	4.1	4.4	3.2	6.8
Equivalent Elastic Deformation	%	33	31	44	42

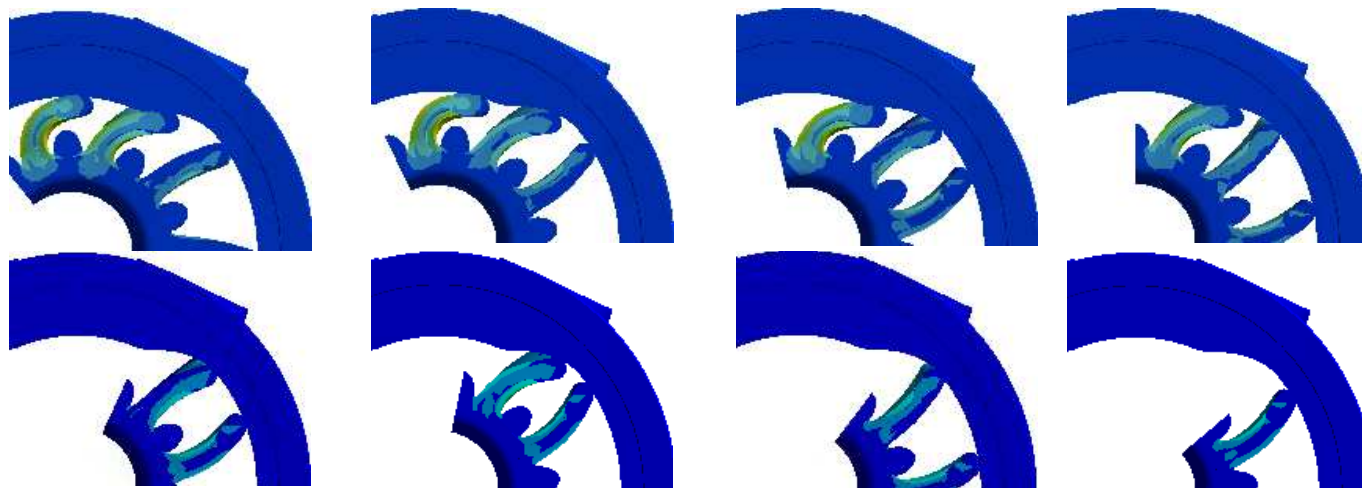


Fig. 15. Blades' evolution during the inversion of motion (strains are shown).

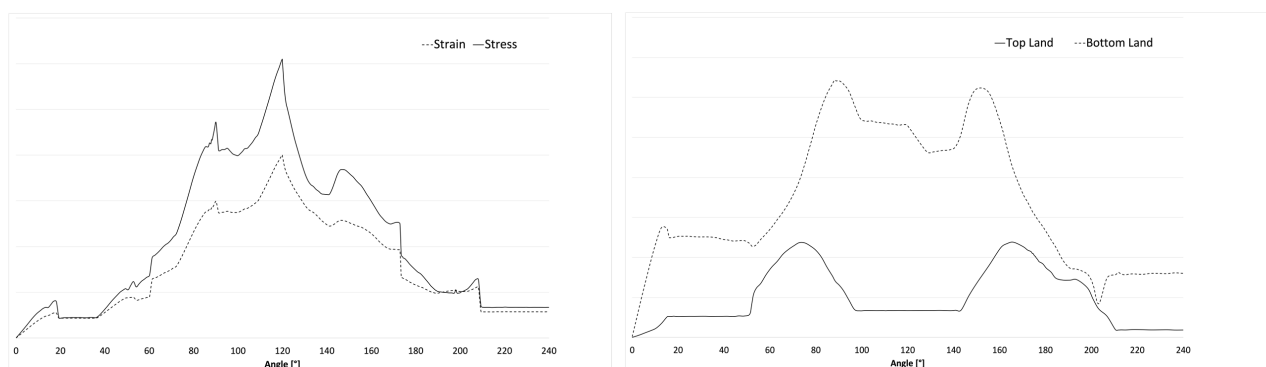


Fig. 16. Stress state during the inversion of motion in terms of maximum values of a) (main) stress and strain; b) stress in the blade's top land and bottom land.

3.5 Material changes

The effect of material changes was investigated for both materials of interest (DA1104 and FP1161, both selected based of the company's needs in terms of Maximum Equivalent von Mises stress, Maximum Principal Stress, Equivalent Elastic Deformation. In no case the stress, always below 6.8 MPa, approach the strength limits of materials, respectively 12.2 and 11.5 MPa (Table 3). From Table 3, it appears that the two different materials have an opposite qualitative behaviour with respect to maximum stress, when comparing direct and inverse motion of the impeller. Therefore, as expected, the impeller is oversized (safety factor > 2), regardless the preferred materials, with respect to quasistatic stresses, although worsened by the application of additional loads (with the scope to replace CFD and centripetal effects), while it should be verified in terms of fatigue. About this, with respect to a fatigue analysis and also the fact that only the stress detected during the direct motion can be associated with this type of validation (since the inversion of the motion is quite infrequent), values of 1.5 MPa and 2.9 MPa could be suggested for the mean and alternating stress components, respectively.

4. Conclusion

This study aimed to develop a simplified finite element (EF) model capable of predicting the trend of deformations and stresses in the different points of a flexible impeller during its operating cycle. Starting from the geometric characteristics of a pump already available on the market, the quasistatic behaviour of the impeller in its rotational movement inside the pump body was simulated by Ansys Workbench. They have been identified, in particular, the values of stress (main and equivalent) and of deformation assumed in the various points of the impeller, both during a normal rotation cycle, which in the presence of a sudden reversal of the movement. The modeling, which had to consider aspects such as the hyperelasticity of the material, the large displacements, the large deformations, and the non-linearity in the contacts, exploited methods of numerical analysis that were not fully consolidated. For example, it has been necessary to use geometrical symmetries in an unusual way, not only to



simplify the system, but also to take account of the pre-deformation of the impeller linked to the procedures of mounting. The results were finally used as analysis tools to evaluate the effects of geometric or material design changes. The future work will take in consideration potential application for further accurate analysis of the dynamics of this kind of Self-Priming Pump, which in any case represents a very challenging issue. Not only for a 'local' analysis (i.e., stress analysis of a rotating blade, taking into account impact forces and viscoelastic behaviour of the material), but also for a 'global' analysis, from the point of view of rotor dynamics. The present work may be very useful as a basis for developing simplified models of the whole rotating pump system (characterized by time-varying coefficients, periodic, or quasi-periodic), for studying specific aspects in the rotor dynamic field.

Author Contributions

Not applicable.

Acknowledgments

The author acknowledges Isopren Srl, Cusano Milanino (Italy) for providing information regarding the material mechanical hyperelastic behaviour. Special thanks to Prof. G. Minak for enabling this study to be initiated.

Conflict of Interest

The author declared no potential conflicts of interest concerning the research, authorship, and publication of this article.

Funding

This investigation was realized thanks to support of Francesca Pompe Enologica Srl, Imola (Italy) that also provided 3D pump parts models together with all information regarding the system working conditions. However, the company had no direct role in the present investigation, analysis of results or in paper writing.

Data Availability Statements


The datasets generated and/or analyzed during the current study are available from the corresponding author on reasonable request.

References

- [1] Phillips, C., Pumps for moving juice, must and wine, *Australian and New Zealand Grapegrower and Winemaker*, 622, 2015.
- [2] Hilton, W. H., NO. XVII. Pump for racking wine, *Transactions Society, Instituted at London, for the Encouragement of Arts, Manufactures, and Commerce*, 47, 1828, 160-162.
- [3] Hilton, W. H. No. III. Pump for racking wine, *Transactions Society, Instituted at London, for the Encouragement of Arts, Manufactures, and Commerce*, 48, 1830, 70-72.
- [4] Astall, R., Pumping wine-look for a happy marriage of speed and geometry, *Australian Grapegrower and Winemaker*, 373, 1995, 21-23.
- [5] Kanute, J., Self-priming centrifugal pumps: a primer, *World Pumps*, 456, 2004, 30-32.
- [6] Wang, C., He, X., Zhang, D., Hu, B., Shi, W., Numerical and experimental study of the self-priming process of a multistage self-priming centrifugal pump, *International Journal of Energy Research*, 43(9), 2019, 4074-4092.
- [7] Wang, C., Shi, W., Wang, X., Jiang, X., Yang, Y., Li, W., & Zhou, L., Optimal design of multistage centrifugal pump based on the combined energy loss model and computational fluid dynamics, *Applied Energy*, 187, 2017, 10-26.
- [8] Li, X., Gao, P., Zhu, Z., Li, Y., Effect of the blade loading distribution on hydrodynamic performance of a centrifugal pump with cylindrical blades, *Journal of Mechanical Science and Technology*, 32(3), 2018, 1161-1170.
- [9] Chang, H., Li, W., Shi, W., Liu, J., Effect of blade profile with different thickness distribution on the pressure characteristics of novel self-priming pump, *Journal of the Brazilian Society of Mechanical Sciences and Engineering*, 40(11), 2018, 1-20.
- [10] Mastrogiannakis, I., Vosniakos, G.-C., Exploring structural design of the francis hydro-turbine blades using composite materials, *Facta Universitatis-Series Mechanical Engineering*, 18(1), 2020, 43-55.
- [11] Spasic, Z., Jovanovic, M., Bogdanovic-Jovanovic, J., Milanovic, S., Numerical investigation of the influence of the doubly curved blade profiles on the reversible axial fan characteristics, *Facta Universitatis-Series Mechanical Engineering*, 18(1), 2020, 57-68.
- [12] Wang, K., Zhang, Z., Jiang, L., Liu, H., Li, Y., Effects of impeller trim on performance of two-stage self-priming centrifugal pump, *Advances in Mechanical Engineering*, 9(2), 2017, 1-11.
- [13] Gu, D., Liu, Z., Xie, Z., Li, J., Tao, C., Wang, Y., Numerical simulation of solid-liquid suspension in a stirred tank with a dual punched rigid-flexible impeller, *Advanced Powder Technology*, 2810, 2017, 2723-2734.
- [14] Gu, D., Liu, Z., Quig, F., Li, J., Tao, C., Wang, Y., Design of impeller blades for efficient homogeneity of solid-liquid suspension in a stirred tank reactor, *Advanced Powder Technology*, 2810, 2017, 2514-2523.
- [15] Yenigun, B., Gkouti, E., Czekanski, A., Barbaraci, G., Jankowski, K.P., Comparison of Elasto-Mechanical Behaviour of Rubbers, in *Proc. of the Canadian Society for Mechanical Engineering International Congress*, June 21-24, Charlottetown, PE, Canada, 2020.
- [16] Bhowmick, A.K., Stephens H., *Handbook of elastomers*, CRC Press, 2000.
- [17] Schaefer, R.J., *Mechanical properties of rubber*, Harris' Shock and Vibration Handbook, Sixth edition, Piersol, A. Paez T. (Eds), McGraw-Hill Companies Inc, 2010.
- [18] Yenigun, B., Gkouti, E., Czekanski, A., Barbaraci, G., Jankowski, K.P., Comparison of Elasto-Mechanical Behaviour of Rubbers, in *Proc. of the Canadian Society for Mechanical Engineering International Congress*, June 21-24, Charlottetown, PE, Canada, 2020.
- [19] Gajewski, M., Szczerba, R., Jemiolo, S., Modelling of elastomeric bearings with application of Yeoh hyperelastic material model, *Procedia Eng.*, 111, 2015, 220-227.
- [20] Constantinou, M.C., Caccese, J., Harris, H.G., Frictional characteristics of Teflon-steel interfaces under dynamic conditions, *Earthquake Engineering & Structural Dynamics*, 15(6), 1987, 751-759.
- [21] Bueche, A.M., Flom, D.G., Surface friction and dynamic mechanical properties of polymers, *Wear*, 2(3), 1959, 168-182.
- [22] Pavlovic, A., Fragassa, C., Geometry optimization by fem simulation of the automatic changing gear, *Reports in Mechanical Engineering*, 1(1), 2020, 199-205.
- [23] Pavlovic, A., Sintoni, D., Fragassa, C., Minak, G., Multi-objective design optimization of the reinforced composite roof in a solar vehicle, *Applied Sciences*, 10(8), 2020, 2665.
- [23] Zhan, J., Fard, M., Jazar, R., A quasi-static FEM for estimating gear load capacity, *Measurement*, 75, 2015, 40-49.
- [24] Altenbach, H., Eremeyev, V., Levdokymov, M., On the impact on a plate made of hyperelastic foam, in *Proceedings of the 3rd International Conference on Nonlinear Dynamics*, Kharkov, Ukraine, 2010.



ORCID iD

Ana Pavlovic  <https://orcid.org/0000-0003-2158-1820>



© 2022 Shahid Chamran University of Ahvaz, Ahvaz, Iran. This article is an open access article distributed under the terms and conditions of the Creative Commons Attribution-NonCommercial 4.0 International (CC BY-NC 4.0 license) (<http://creativecommons.org/licenses/by-nc/4.0/>).

How to cite this article: Pavlovic A., Finite Elements Analysis of the Hyperelastic Impeller Rotating in the Self-Priming Pump, *J. Appl. Comput. Mech.*, 8(3), 2022, 1103–1112. <https://doi.org/10.22055/jacm.2022.39750.3457>

Publisher's Note Shahid Chamran University of Ahvaz remains neutral with regard to jurisdictional claims in published maps and institutional affiliations.

